

Article

Mechanical Properties and Numerical Analysis of Underground Continuous Wall in Underground Grain Silo Foundation Pit

Chen Zhao ¹, Yong Feng ², Weijian Wang ^{2,*} and Zijuan Niu ²

¹ Department of Hydraulic Engineering, Henan Vocational College of Water Conservancy and Environment, Zhengzhou 450008, China

² College of Civil Engineering and Architecture, Henan University of Technology, Zhengzhou 450001, China

* Correspondence: 2021920250@stu.haut.edu.cn

Abstract: Foundation pit monitoring can only provide feedback regarding the deformation of the formation and envelope structure after construction, and it is difficult to predict the deformation law of a continuous underground wall in the later stage of underground grain silo support. Taking the deep foundation pit of a continuous underground wall of an underground grain silo as an example, this paper uses Abaqus software to simulate the force of the project, explores the calculation results of the planar elastic foundation beam considering the arch effect and the numerical simulation technology of the foundation pit's support, and analyzes and compares the rationality of the model. The analysis of the deformation form of the continuous underground wall by both calculation methods is a parabolic combination. The maximum horizontal displacement of the continuous underground wall, according to the Abaqus software, is 6.23 mm, and the other calculation result is 4.7 mm; the maximum settlement on the surface is 11.34 mm, according to the Abaqus software, and the other maximum settlement is 8 mm. The simulation results show that the simulated value is basically consistent with the measured value, and the simulated value is slightly larger than the measured value because the interference conditions are idealized during simulation. The accuracy and rationality of the numerical simulation are verified, and the parameters, such as the thickness and burial depth of the continuous underground wall, can be changed to provide a reference for the support method of a deep foundation pit similar to a continuous underground wall.



Citation: Zhao, C.; Feng, Y.; Wang, W.; Niu, Z. Mechanical Properties and Numerical Analysis of

Underground Continuous Wall in Underground Grain Silo Foundation Pit. *Buildings* **2023**, *13*, 293. <https://doi.org/10.3390/buildings13020293>

Academic Editor: Ahmed Senouci

Received: 6 December 2022

Revised: 25 December 2022

Accepted: 3 January 2023

Published: 19 January 2023



Copyright: © 2023 by the authors. Licensee MDPI, Basel, Switzerland. This article is an open access article distributed under the terms and conditions of the Creative Commons Attribution (CC BY) license (<https://creativecommons.org/licenses/by/4.0/>).

Keywords: diaphragm wall; foundation pit support; numerical simulation

1. Introduction

Diaphragm wall technology is a common enclosure structure used in support of a deep foundation pit, which can effectively use the spacing effect of the foundation pit. The supporting structure of the foundation pit is optimized to produce a good engineering effect. In the current construction of granaries, underground granaries have great development prospects because they are in a low-temperature environment underground; it is therefore not easy for the stored grain to incur insects, thereby reducing the cost of grain storage. Secondly, an underground granary can effectively alleviate the problem of land resource tension. Finally, lower granaries have anti-seismic functions. Even in extreme situations such as earthquakes and wars, they can better preserve food to ensure our safety and China's food security.

In order to ensure the safety of the foundation pit and the surrounding environment, a monitoring method is usually adopted to master the deformation state of the supporting structure. Nonetheless, foundation pit monitoring can only provide feedback on the deformation of the stratum and enclosure structure after construction in real time and judge whether it exceeds the safety warning value, which is difficult to predict in the later stage of structural deformation laws. To reasonably predict and ensure the safety and development of the diaphragm wall in the foundation pit support of the underground

granary, a foundation pit excavation model is built based on field measurements and numerical software. According to the geological and hydrological construction conditions, the soil parameters are assigned to the model. Finally, through the simulation calculation of the process, interaction, and boundary conditions in the process of the foundation pit excavation, one must analyze the distribution of soil displacement and stress during the excavation of the foundation pit, predict its change trend, and evaluate the structural reliability. Many scholars use theoretical analysis [1,2], field measurements [3–5], model tests [6–9], and numerical simulations [10] to solve this problem. Abaqus is an engineering simulation finite element software that can analyze complex nonlinear problems. Wang Shaojun et al. [11], Guo Xueyuan et al. [12], and Li et al. [13] used Abaqus to simulate the whole process of the foundation pit excavation, analyzed the changes in horizontal displacement and internal force of the support structure, and verified that Abaqus simulates the excavation of a foundation pit and studies the reliability of deformation problems. Due to the strong practicability and remarkable enclosure of the diaphragm wall, studies regarding diaphragm walls and internal supports of the enclosure structure system have never stopped. Ren Dongxing et al. [14] used the ultra-deep TRD method to measure and analyze the deformation of the building foundation pit retaining structure and the supporting force. Through three-dimensional finite element analysis, Zhou Peidong et al. [15] determined that a diaphragm wall support scheme with a long- and short-amplitude combination can effectively reduce the difficulty of constructing a rock-socketed section of a diaphragm wall. Liu Xu et al. [16] conducted a numerical simulation of the foundation pit excavation process through Abaqus and analyzed the variation characteristics of the horizontal displacement of the diaphragm wall with depth during foundation pit construction. Wang Xianian et al. [17] and Chen Yang et al. [18] analyzed the deformation characteristics of deep foundation pit construction in pebble and sandy soil layers based on field measurement and numerical simulation methods. Wu Changjiang et al. [19] studied the deformation characteristics induced by the construction of a continuous underground wall foundation pit and its influence on adjacent buildings based on the actual measurement results of a continuous underground wall foundation pit in a soft soil area. He Shaoheng et al. [20] used numerical simulation methods to study the coupling law of seepage and deformation of the foundation pit of a suspended water-stop curtain under the action of precipitation seepage. Hu Yong et al. [21] analyzed the deformation law of foundation pits under the conditions of water level pressure changes with the help of model experiments and numerical simulation methods to study the influence of foundation pit size and pressurized water height on the three-dimensional spatial effect of foundation pits. However, there is little research on continuous underground walls supporting underground granary foundation pits.

Taking an underground grain silo project as the engineering background and using its geological situation as the analysis basis, the support scheme selects the continuous underground wall and the inner support enclosure method and studies the design and calculation method of underground grain silo foundation pit engineering using underground continuous wall technology as the support method. This article also studies the dynamic construction process by numerical simulation of the underground grain silo foundation pit support through Abaqus so as to calculate the deformation and force of the foundation pit and support and monitor deep changes in horizontal displacement of the continuous underground wall in real time during the construction process. Compared with the calculation results of the plane foundation beam method, the monitoring data and numerical simulation results are compared and analyzed, and the accuracy of the results and the rationality of the model are verified, which provides a reference for a method of supporting deep foundation pits similar to continuous underground walls, which has a certain positive effect on promoting the construction and development of an underground granary, and promotes the development of “two walls in one” technology of a continuous underground wall support in engineering. The technology research roadmap is shown in Figure 1.

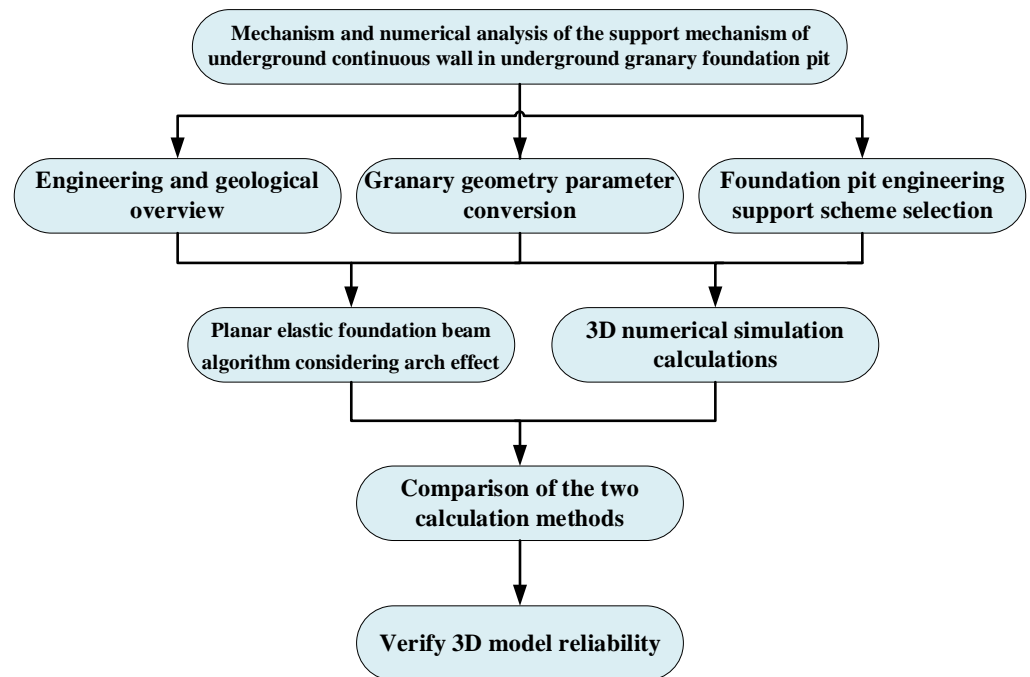


Figure 1. Technology roadmap.

2. Project Overview

2.1. Project and Geological Overview

In Figure 2a,b, the stratum distribution of this project's foundation pit site for an underground granary building project is depicted. According to the building's design, which is seen in Figure 3, the underground grain storage facility has a storage capacity of 5000 t, a diameter of 24.00 m, and a depth of 22.00 m (including the inverted conical bottom structure with a depth of 6 m). The self-waterproof concrete used to construct the warehouse body has an impermeability grade of P12.

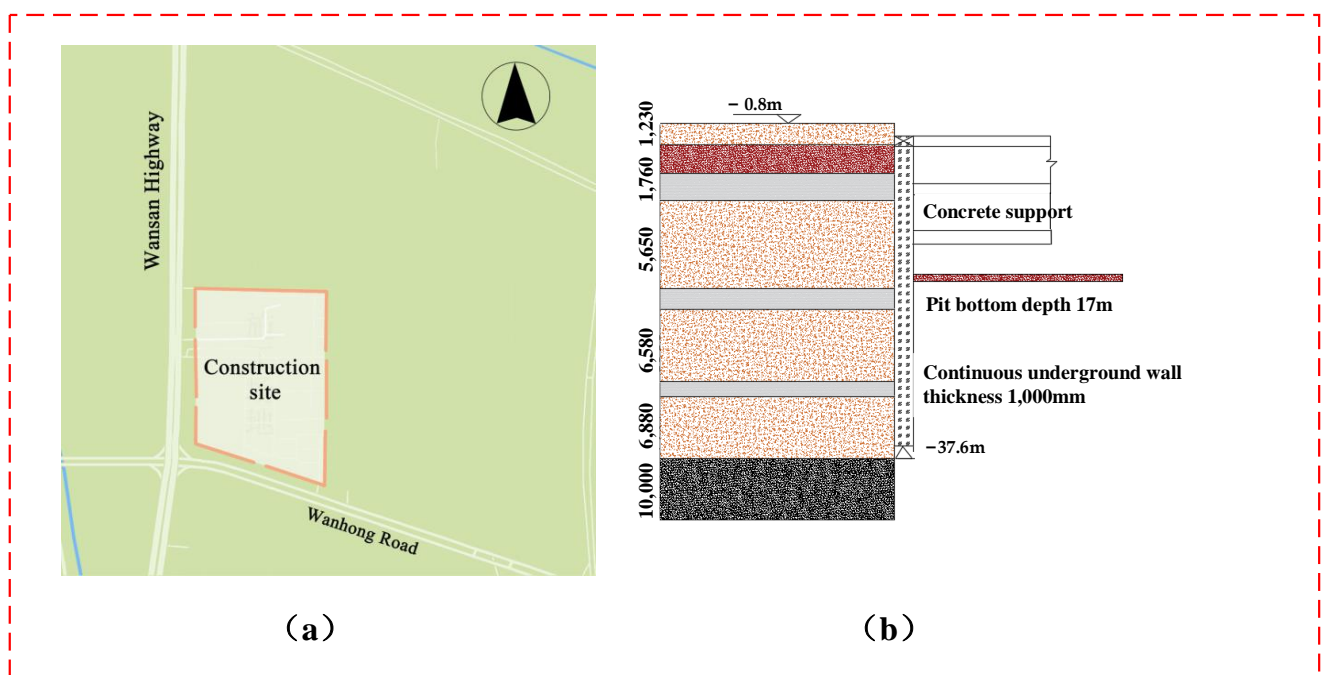


Figure 2. Engineering and geology overview: (a) construction site map; (b) stratigraphic map.

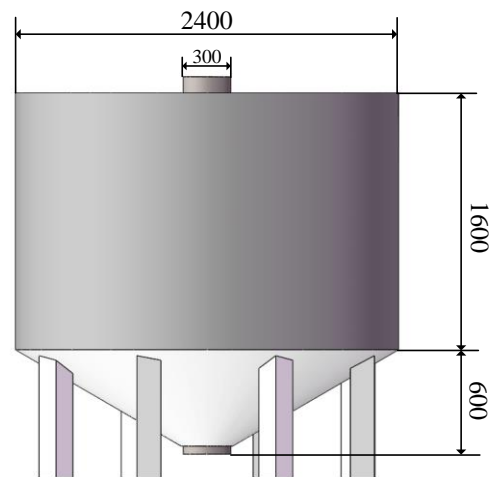


Figure 3. Granary structure diagram.

2.2. Conversion of Geometric Parameters at the Bottom of Underground Granary

The inverted cone foundation pit, which has a bottom depth of 6 m, significantly enhances the calculation and computational difficulty. A specific amount of conversion is performed since the cost is calculated. Here is the precise conversion procedure:

(1) Calculating the grade of the slope at the bottom of the foundation pit:

$$\tan \beta = 6 / (1)12 = 0.5, \quad (1)$$

$$\beta = \arctan 0.5 = 26.565^\circ, \quad (2)$$

(2) According to the geological survey report, the soil layer at the bottom is determined to be a fine sand layer:

$$c = 0 \text{ kPa}, \phi = 22^\circ, \quad (3)$$

c is cohesion; ϕ is the internal friction angle.

(3) Conical slope stability assessment:

A cylindrical inverted cone slope model with a height of 6 m, a bottom radius of 12 m, a bottom radius of 36 m, and a height of 18 m is built as the basic soil model using the Abaqus program as the calculation platform. The strength reduction analysis phase is established after choosing the Mohr–Coulomb constitutive relationship for the soil. At the location variable of 1.9, a clear turning angle is present. Since $K = 1.9 > 1$ is an acceptable value and the inverted cone slope is stable, it can be converted.

(4) Transform the bottom cone into a cylinder with an equal bottom surface and volume, where the converted cylinder height equals the estimated depth of the inverted cone's bottom:

$$H = \frac{V}{S} = \frac{1}{3} h = \frac{1}{3} \times 6 = 2 \text{ m}, \quad (4)$$

The foundation pit for this project is shaped like a cone with a bottom height of 6 m and a cylinder with an upper height of 16 m. Engineering knowledge and calculations indicate that the calculation model can be transformed into a cylinder foundation pit model with a depth of 18 m.

2.3. Foundation Pit Engineering Support Scheme Selection

The project's overarching support design plan employs the top-down methodology. Most of the soil used for the project is silty sand with poor cohesiveness. The excavation is 18 m deep. The foundation pit is circular, creating the appearance of an arch [22]. As a result, adopting a self-supporting support system is proposed. A diaphragm wall cast in situ is chosen as the enclosure structure because it not only uses the circular foundation pit's arch effect to support the pit evenly and continuously, but it also uses the compressive

properties of concrete to effectively convert lateral water and soil pressure into circumferential pressure. The circular diaphragm wall's properties are taken into consideration when choosing the lining wall as the support. The final scheme is as follows: reverse construction + diaphragm wall support + lining wall.

3. Calculation of Plane Elastic Foundation Beam Considering Arch Effect

3.1. Calculation of Lateral Pressure

The static earth pressure and lateral pressure are calculated as follows:

$$p = K\gamma z, \quad (5)$$

$$E = \frac{1}{2}\gamma H^2 K, \quad (6)$$

$$K = \begin{cases} 1 - \sin \phi' & (\text{Sandy soil}) \\ 0.95 - \sin \phi' & (\text{Cohesive soil}) \end{cases} \quad (7)$$

$$\phi' = 0.7(c + \varphi), \quad (8)$$

$$P = \begin{cases} K\gamma z, & \text{Above the water table} \\ K[\gamma h + \gamma'(z - h)] + \gamma_w(z - h), & \text{Below the water table} \end{cases} \quad (9)$$

Since the building site's groundwater level is 1 m, the lateral pressure distribution of each layer can be computed using this formula, and the total foundation pit support structure's lateral pressure distribution can then be synthesized.

3.2. Internal Force Calculation of Continuous Wall

This research optimizes the plane elastic foundation beam method, taking into account the arch effect by internal force analysis of the diaphragm wall [23]. Its calculating method is to discretely transform the space arch effect of a circular foundation pit into a spring support and then calculate using the spring support, as shown in Figure 4.

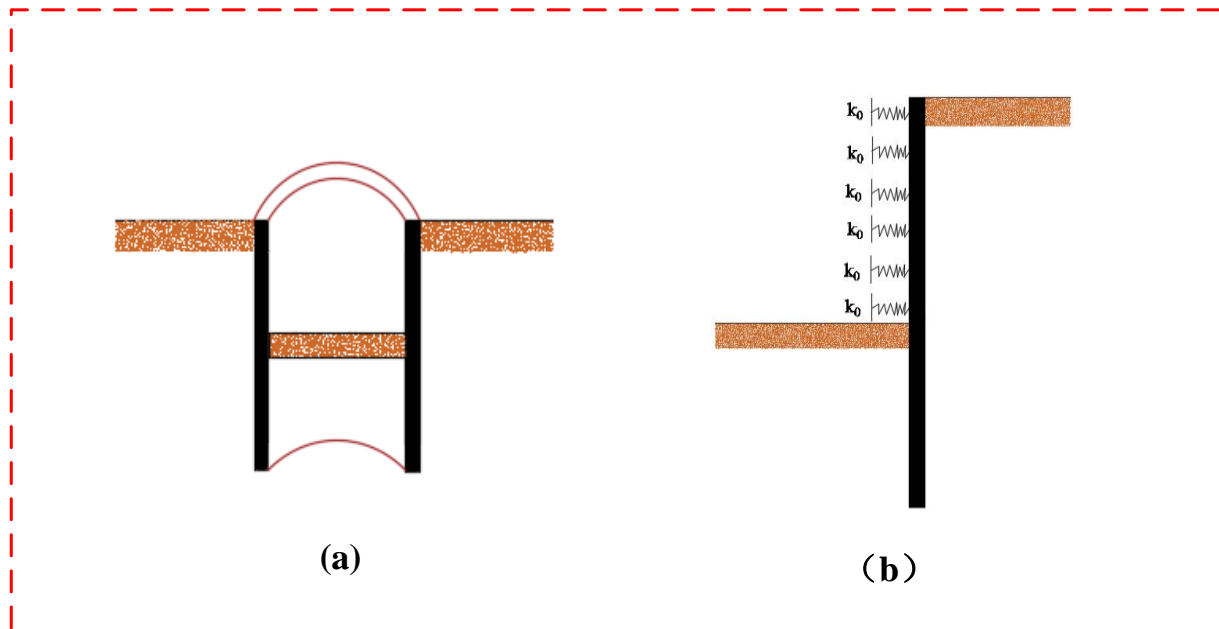


Figure 4. Schematic diagram of calculation of underground diaphragm wall support: (a) schematic diagram of support; (b) schematic diagram of arch effect conversion.

According to Hooke's law, the resistance of soil mass to the diaphragm wall can be computed as follows:

$$\sigma_z = k_s y, \quad (10)$$

where σ_z is the soil resistance of the diaphragm wall structure (KN/m^2); k_s is the horizontal subgrade bed coefficient of the foundation (KN/m^3); y is the horizontal deformation of the soil mass (m).

For the purpose of calculating and analyzing the internal force of the retaining structure of the foundation pit, the arch effect of the two walls can be compared to the support loading on the diaphragm wall. Adopt the procedure method:

$$K = E_1 b / \rho^2, \quad (11)$$

In the formula, E_1 is the circumferential elastic modulus of the diaphragm wall, $E_1 = \alpha E$; E is the elastic modulus of the diaphragm wall; α is the corresponding reduction coefficient; b is the wall thickness; ρ is the average radius.

3.3. Calculation Results

According to the calculation accuracy standards of this project, the effect is equivalent to a vertical spacing of the inner support of 1 m, and the stiffness coefficient of the spring support is equivalent to an arch effect of 1 m in height. The method of calculation is as follows:

(1) Calculation of equivalent stiffness of diaphragm wall in space effect

$$K_1 = E_1 b / \rho^2 = 22,750 \times 1 / 12.9^2 = 136.7 \text{ mN/m}, \quad (12)$$

In the formula, C40 is selected for concrete, the elastic modulus is 32,500 MPa, and the reduction coefficient based on experience α 0.7 is selected, so the circumferential elastic modulus is as follows:

$$E_1 = \alpha E = 22,750 \text{ MPa}, \quad (13)$$

The radius ρ is the equivalent radius, which is the average of the outer and the inner diameters:

$$\rho_1 = (r_1 + r_2) / 2 = (13.4 + 12.4) / 2 = 12.9 \text{ m}, \quad (14)$$

(2) Calculation of Equivalent Stiffness of Inner Wall Space Effect

$$K_2 = E_2 b / \rho^2 = 21,000 \times 0.4 / 12.2^2 = 56.4 \text{ mN/m}, \quad (15)$$

In the design, C30 concrete is used for the lining wall, the elastic modulus is MPa, the reduction coefficient α is still 0.7, and the circumferential elastic modulus is still selected, as follows:

$$E_2 = \alpha E = 21,000 \text{ MPa}, \quad (16)$$

radius:

$$\rho_2 = (r_2 + r_3) / 2 = (12.4 + 12) / 2 = 12.2 \text{ m}, \quad (17)$$

(3) The shrinkage changes of the inner lining wall and the diaphragm wall are not coordinated because of the differing masonry times; thus, there will be a trend of separation. Before the first lining wall is built in the foundation pit, a top ring beam with a cross section of 1500 mm \times 1000 mm is poured. It is necessary to first make the ring beam spring support equivalent when using the Lizheng deep foundation pit software for calculation. The equivalent stiffness is as follows:

$$K_3 = E_1 A / \rho^2 = 22,750 \times 1.5 / 12.65^2 = 213.3 \text{ mN/m}, \quad (18)$$

Among them, the selection of the concrete model and reduction coefficient is consistent with that of the diaphragm wall, so the circumferential elastic modulus:

$$E_1 = 22,750 \text{ MPa}, \quad (19)$$

radius ρ is the average of the equivalent radius, i.e., the outer diameter and the inner diameter

$$\rho_3 = (r_1 + r_4) / 2 = (13.4 + 11.9) / 2 = 12.65 \text{ m}, \quad (20)$$

When the equivalent bracing parameters are entered into the deep foundation pit software, 18 virtual bracing cases must be added to the original working conditions. The arch effect of the diaphragm wall begins to occur in the foundation pit project after the pouring and before the excavation of the foundation pit. As a result, when the project is calculated using Lizheng deep foundation pit software, the structural calculation of the diaphragm wall is performed after the virtual support working condition is added. After the continuous underground wall is poured into the excavation of the foundation pit, the continuous underground wall has little effect on the water and soil pressure; in the theoretical situation where the inside and outside of the wall are balanced, at this time, the displacement and internal force are zero. After the excavation of the foundation pit, the displacement, bending moment, and shear force of the supporting structural change in Figure 5a–c are the result of the elastic foundation beam algorithm; observing the displacement and internal force change diagram of the supporting structure excavated by the foundation pit, it can be seen from the change in the figure that in the initial stage of the excavation of the foundation pit, the supporting structure is deformed into a cantilever type. With the excavation of the foundation pit and the addition of support, the deformation of a continuous underground wall gradually takes the form of a parabolic combination, meaning that the horizontal displacement in the middle of a continuous underground wall is the largest and the horizontal displacement at the bottom is the smallest. This means that the horizontal displacement at the top of the foundation pit support structure is the largest. It can be seen from the figure that after the excavation of the foundation pit, the maximum displacement is in the middle of a continuous underground wall, the value is 4.7 mm, the maximum bending moment is $-279.25 \text{ kN}\cdot\text{m}$, and the maximum value is also located in the middle of a continuous underground wall.

3.4. Foundation Pit Stability Calculation

3.4.1. Overall Stability Analysis

To avoid damage to the foundation pit from overall sliding between the support for the foundation pit and the surrounding soil, it is important to examine the foundation pit's overall stability. The Sweden slice approach is used, and Figure 6 displays the check calculation diagram. The width of the dirt strip in this estimate is 0.40 m, which can satisfy the project's requirements. The circle's calculated center is located at (5.290, 11.381), and the arc's radius is 24.213 m. The final number is 1.204 for the overall stability safety factor.

3.4.2. Analysis of Overall Uplift Resistance

The safety of the foundation pit will be threatened if the soil in the excavation pit heaves beyond a specified range owing to unloading during the excavation operation. The stability against heave must therefore be examined. At the moment, engineers in China frequently take into account $c-\phi$ while performing an anti-uplift stability study. In this approach, the foundation is the portion below the bottom of the foundation pit wall, and the uplift stability coefficient is computed using the foundation bearing capacity model. The formula is as follows:

$$K_s = \frac{\gamma DN_q + cN_c}{\gamma(H + D) + q}, \quad (21)$$

The value of N_q has different formulas according to different assumptions:

When the base is assumed to be smooth:

$$N_q = \begin{cases} e^{\pi \tan \phi} \tan^2 \left(\frac{\pi}{4} + \frac{\phi}{2} \right), & \text{(When the base is assumed to be smooth)} \\ \frac{1}{2} \left[\frac{e^{\left(\frac{3}{4} \pi - \frac{\phi}{2} \right) \tan \phi}}{\cos \left(\frac{\pi}{2} + \frac{\phi}{2} \right)} \right]^2, & \text{(When the base is assumed to be rough)} \end{cases}, \quad (22)$$

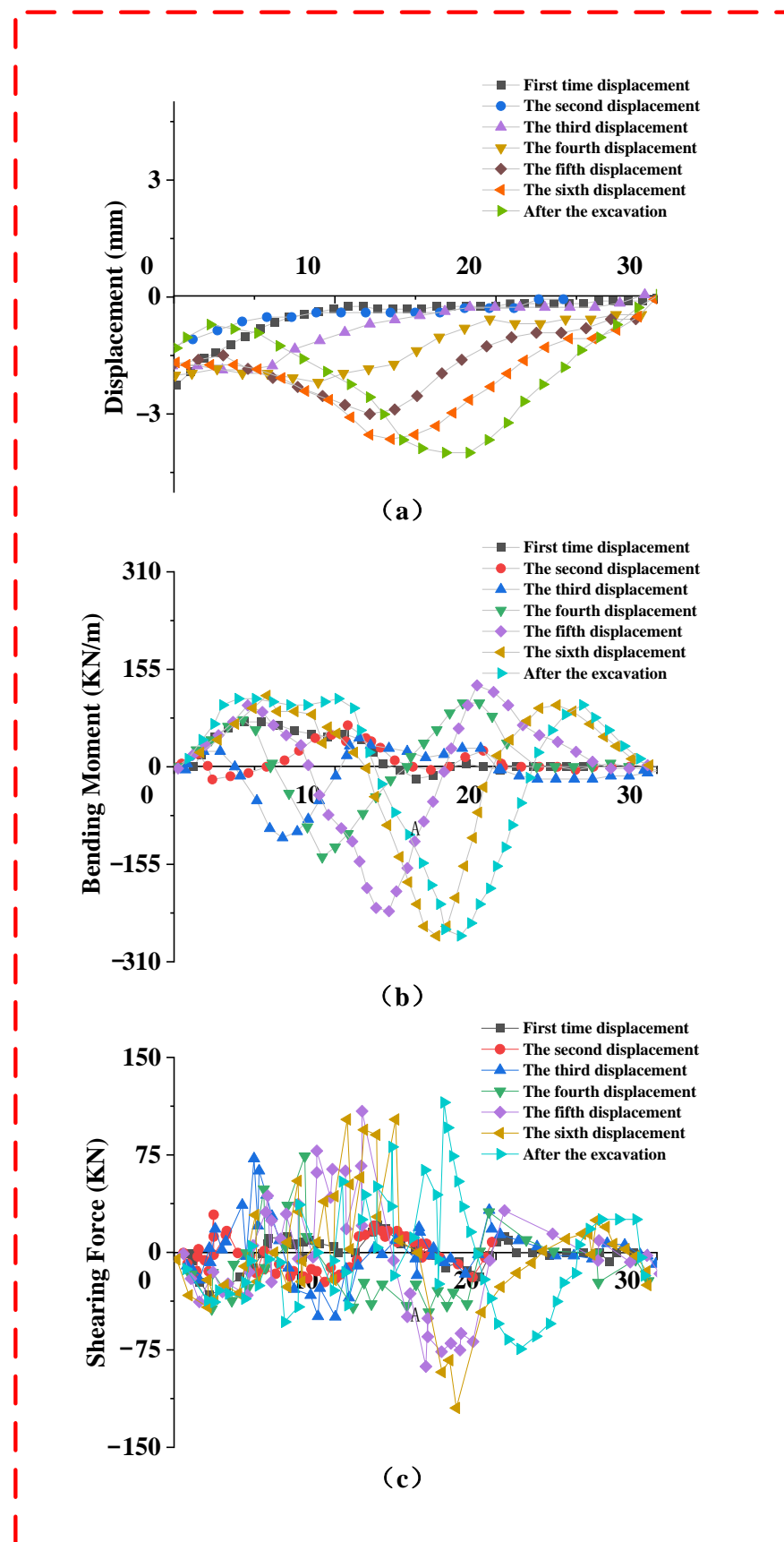


Figure 5. Results of the elastic foundation beam algorithm: (a) displacement map; (b) curved moment diagram; (c) shear diagram.

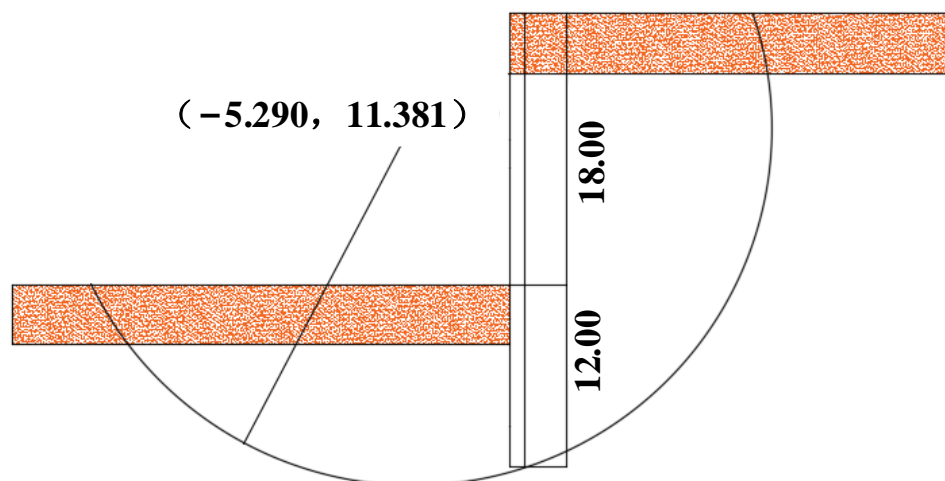


Figure 6. Calculation diagram of foundation pit stability.

The value of N_c is found according to the formula:

$$N_c = (N_q - 1) \frac{1}{\tan \phi}, \quad (23)$$

The calculation results assume that the base is smooth: $K_s = 3.030 \geq 1.1$, meeting the specification requirements; assuming that the base is rough: $K_s = 3.561 \geq 1.15$, meeting the specification requirements. It can be seen that the design scheme meets the anti-uplift checking calculation.

3.4.3. Overall Anti-Overturning Analysis

The anti-overturning stability analysis is a computation used to ensure that the support structure will not topple over. Typically, it is believed that excessive rotation of the support structure around the front toe is what causes overturning [24]. The front toe moment between the support weight and the internal soil pressure is the ratio of the lateral pressure acting on the outside of the foundation pit to the index used to measure stability. According to the specification, the anti-overturning stability safety factor must be larger than 1.3. The calculation's findings show that the minimum safety factor for anti-overturning stability under the worst possible circumstances is 6.024, which satisfies the specification's requirements. As a result, the anti-overturning stability criteria are met by the foundation pit support.

4. Numerical Simulation

The reason why ABAQUS software has only recently been widely promoted and developed is that the application of the method requires a lot of calculations, and in the early days of computer technology, due to the low level of development caused by slow and difficult popularization, it was not possible to perform large-scale computer-aided finite element method calculations, restricting its use to smaller-scale calculations. The finite element method did not start to find increasing use until the quick advancement of computer technology and the creation and promotion of numerous general finite element software.

4.1. Establishment of Numerical Calculation Model

4.1.1. Model Overview

Abaqus modeling is conducted according to the converted cylindrical foundation pit model with a constant section, and the grid element is C3D8.

The Mohr–Coulomb model is one that describes how soil is made. A foundation hole is a symmetrical form, and the soil layer around it is simplified in this work to be a homogeneous soil layer. Therefore, a half cylinder is used to reduce the calculation cost.

The model is constructed and then put together. The tie connects the bottom of the diaphragm wall to the lining wall and the dirt in the foundation pit. The side and the earth are established as friction contact surfaces. The friction coefficient is set to 0.51, and the friction characteristic is configured to be a penalty, as shown in Figure 7.

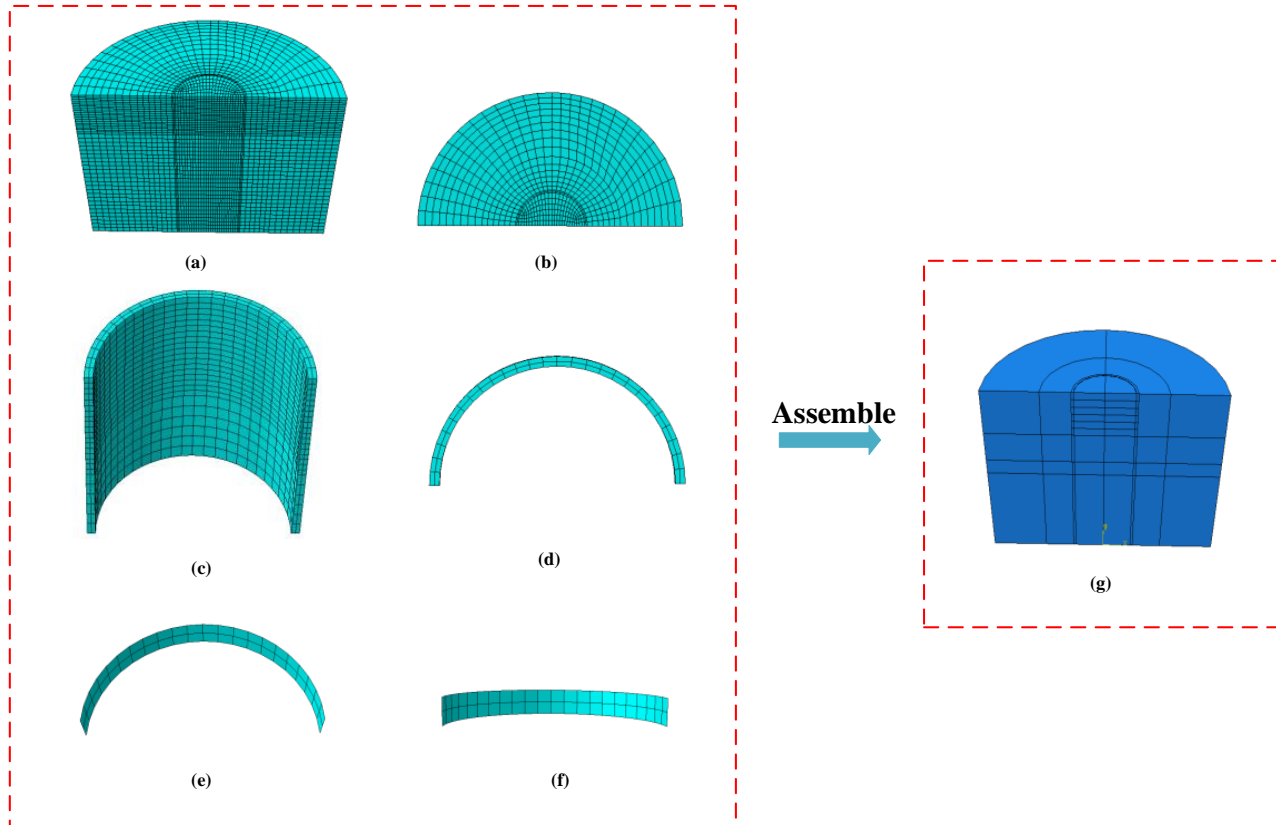


Figure 7. Model assembly renderings: (a) overall view of soil model; (b) top view of soil model; (c) overall drawing of underground diaphragm wall; (d) top view of underground diaphragm wall; (e) overall drawing of lining wall; (f) front view of lined wall; (g) model assembly renderings.

4.1.2. Boundary Conditions and Loads

According to Figure 8, the curved surface of the foundation pit soil restricts the displacement in the x and y directions, the symmetrical section of the foundation pit soil restricts the displacement in the x and y directions, the top of the soil model does not impose constraints, and the bottom of the soil model restricts the displacement in the x, y, and z directions.

4.1.3. In Situ Stress Balance

The soil model deforms after the gravitational field is given to it after it has been simplified as a model. When computing the deformation of the soil model, the geo-stress balance principle aims to augment the deformation brought on by the gravity field.

Figure 9 displays the soil model's stress and displacement program following the application of a gravity field and a geo-stress balance operation. The soil can withstand the stress of up to 280.13 MPa from its gravity. The stress changes from the top to the bottom of the soil body, with the top stress being zero and the bottom stress being the highest, as can be seen after the stress balance. The soil model does not create displacement.

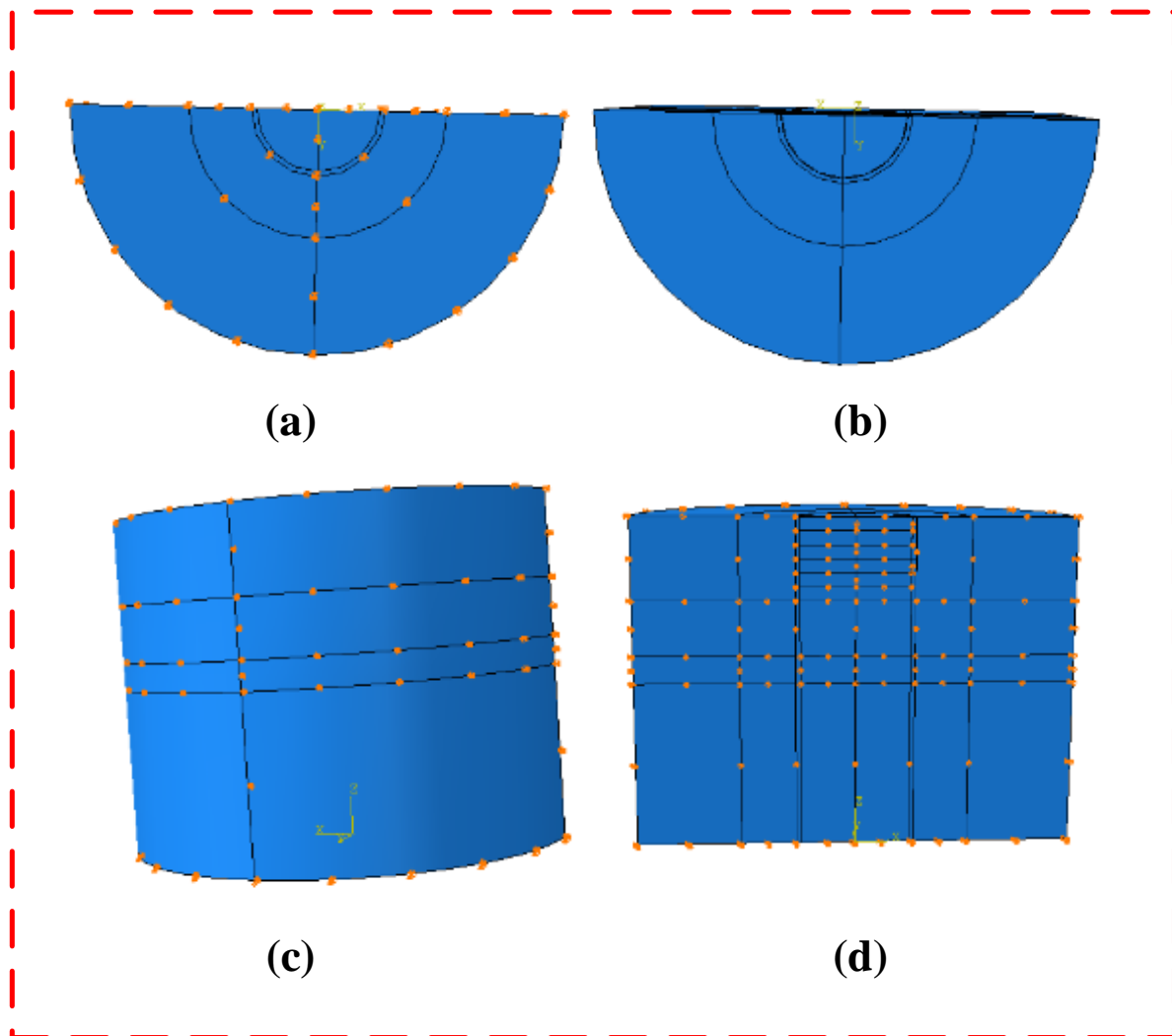


Figure 8. Schematic diagram of model constraints: (a) model bottom constraints; (b) model top constraints; (c) model side constraints; (d) model frontal constraints.

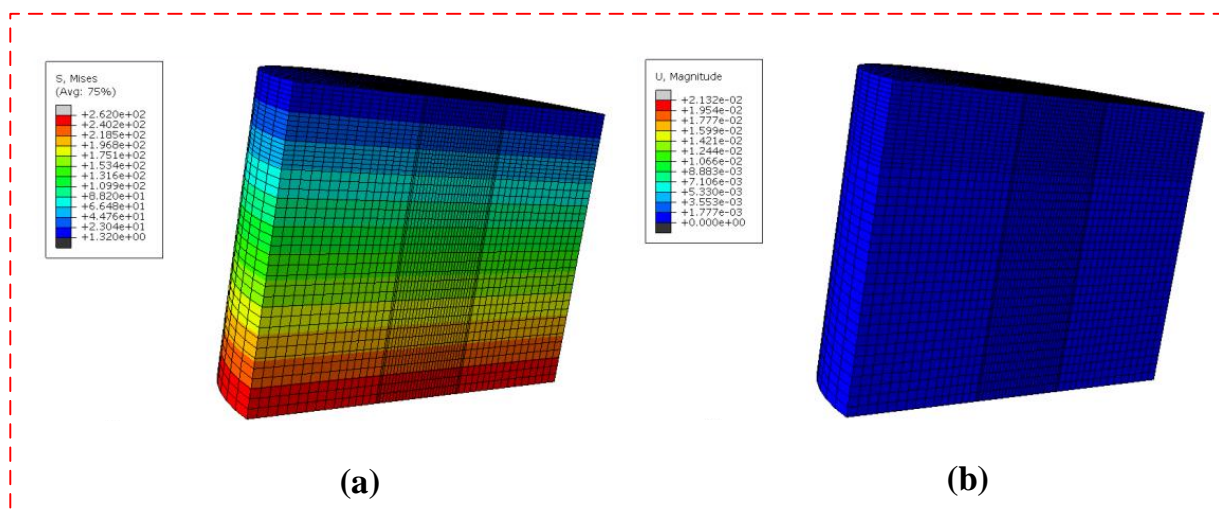


Figure 9. The stress–displacement nephogram after in situ stress equilibrium: (a) stress contour; (b) displacement contour.

4.2. Calculation Results

4.2.1. Foundation Pit Soil Displacement Analysis

Due to unloading, the soil mass will move during the foundation pit excavation, substantially jeopardizing the engineering safety of the pit. Therefore, when designing the foundation pit, the displacement of the soil mass should be tightly controlled. The largest portion of the foundation pit model that is perpendicular to the symmetrical plane is chosen as the observation plane to aid in the investigation of soil displacement. After the first, second, third, fourth, fifth, and sixth soil layers are excavated, the soil displacement of the foundation pit is examined.

Figure 10 depicts the cloud diagram of the vertical displacement of soil mass following the removal of the first, second, third, fourth, fifth, and sixth soil layers. The cloud diagram shows that as the foundation pit's soil layer is continuously excavated, both the vertical displacement amplitude and the vertical displacement of the mass of soil at the bottom of the pit gradually increase. The soil surrounding the foundation pit will also move as a result of unloading. The dirt near the foundation pit will settle during the vertical displacement, and the cloud chart indicates that this settlement will eventually go away as you move away from the foundation pit.

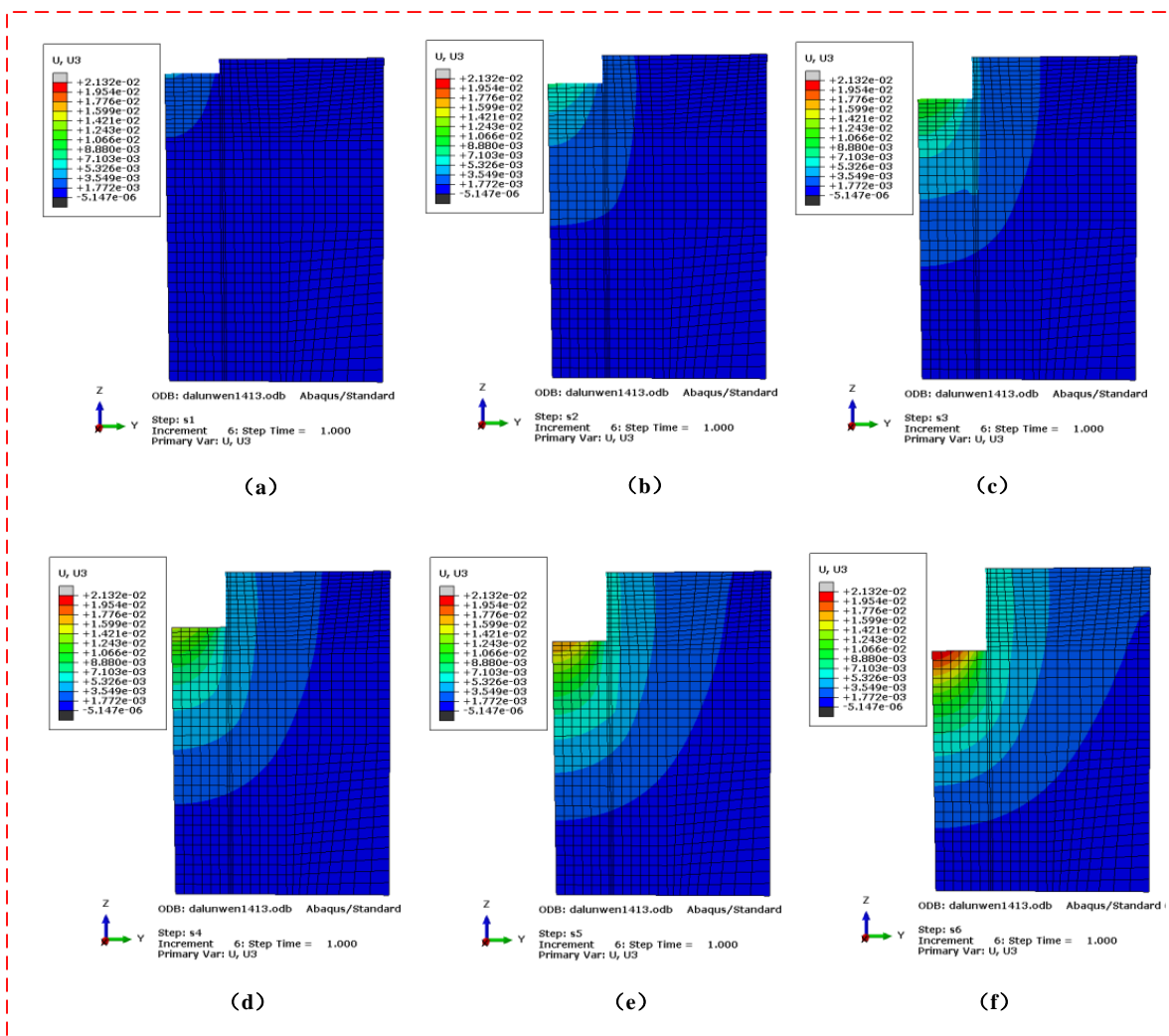


Figure 10. Vertical displacement cloud image of soil: (a) underground first floor; (b) underground second floor; (c) underground third floor; (d) underground fourth floor; (e) underground fifth floor; (f) underground sixth floor.

Figure 11 depicts the timeline for the horizontal displacement of soil mass following the excavation of the first, second, third, fourth, fifth, and sixth soil layers. The program shows that the pit wall of the foundation pit is the area with the most significant horizontal displacement of the soil mass. After the initial excavation, the first layer of soil mass's top is where the movement trend is largest, and as the foundation pit continues to be excavated, the pit wall of the pit moves continuously inward. Later, as the third layer of soil was excavated, the largest displacement was gradually achieved at the excavation surface of the foundation pit. Due to the excavation of the soil layer, the soil in the area surrounding the foundation pit and at its bottom will also move horizontally. As the displacement and affected area increase as a result of the excavation of the soil layer, the displacement will gradually decrease as the direction away from the foundation pit increases.

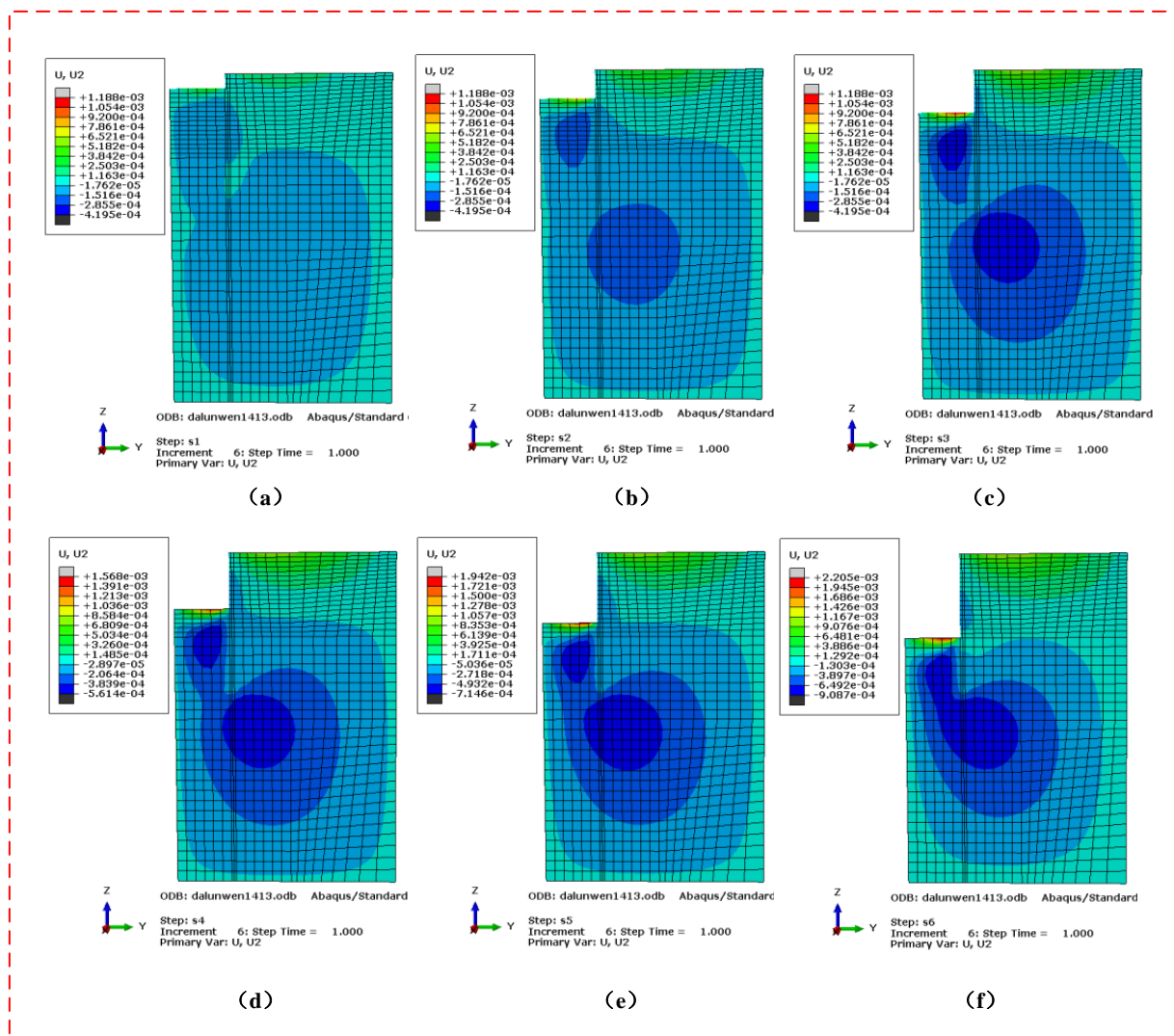


Figure 11. Cloud map of soil's horizontal displacement: (a) underground first floor; (b) underground second floor; (c) underground third floor; (d) underground fourth floor; (e) underground fifth floor; (f) underground sixth floor.

4.2.2. Vertical Displacement Analysis of Foundation Pit Bottom

Figure 12a depicts the soil profile displacement program at 18 m of the top plate of the foundation pit following the excavation of the foundation pit. Following the excavation of the foundation pit, the pit bottom exhibits a relatively obvious vertical deformation, or bulges, which is more noticeable in the foundation pit. The vertical deformation outside the foundation pit is minimal inside the cut plane of the height of the pit bottom and

gradually becomes less the farther distance it is from the foundation pit. Figure 12b depicts the vertical displacement of the foundation pit’s pit bottom following the excavation of each soil layer. As the foundation pit is continuously excavated, the pit bottom heave gradually increases. The highest vertical displacement of the pit bottom occurs once the foundation pit’s excavation is complete. The largest and minimum vertical displacements during this period are 23.4 and 7.1 mm, respectively. The foundation pit’s stability is good, and the project’s pit heave is relatively moderate, as evidenced by the maximum vertical displacement of the pit bottom following the completion of the foundation pit excavation.

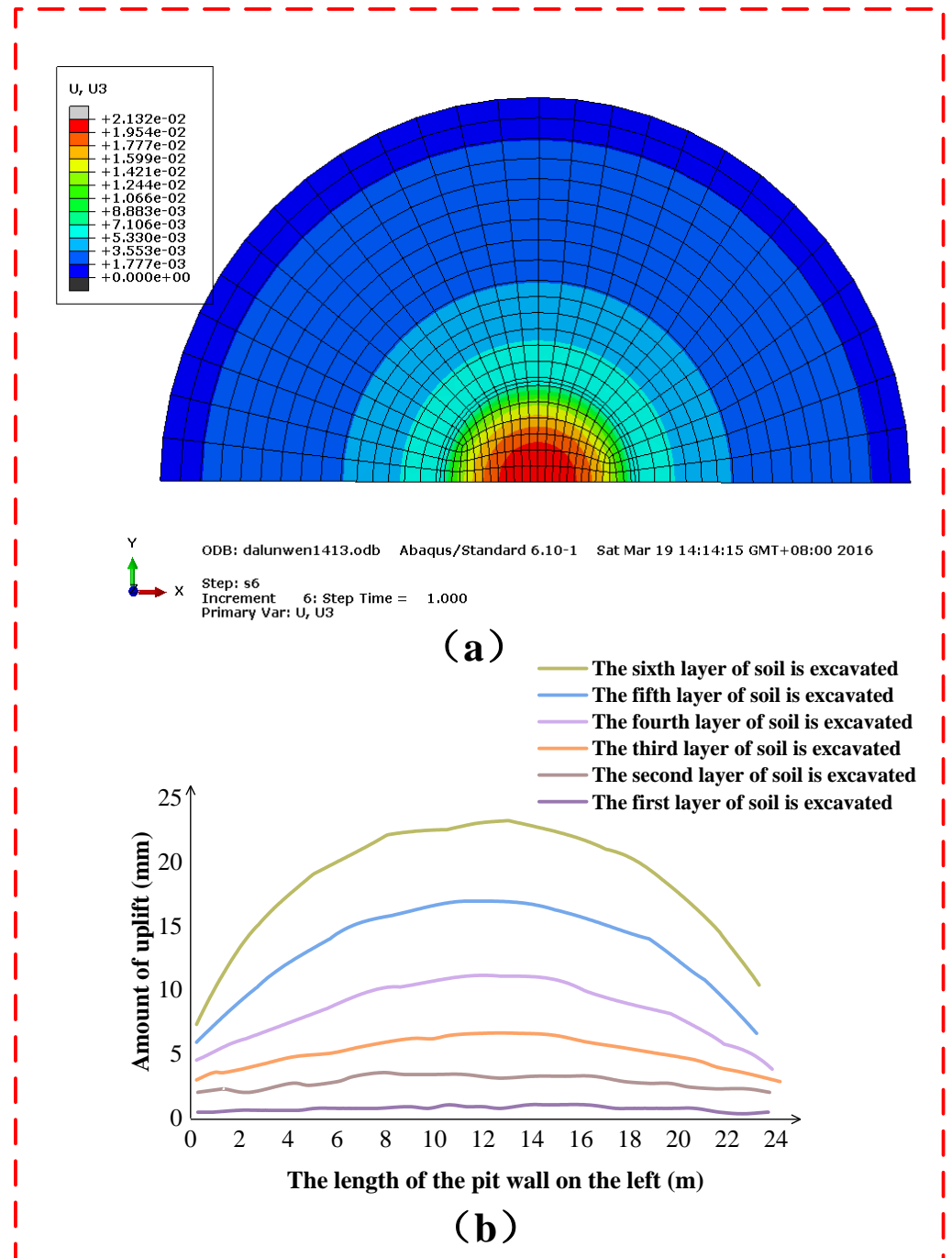


Figure 12. The bottom of the pit: (a) soil profile displacement cloud; (b) pit floor vertical displacement diagram.

4.2.3. Analysis of Surface Settlement Deformation

The ground surrounding the foundation pit will subside when the surrounding soil moves throughout the excavation process. The cloud map of the ground's vertical displacement is shown in Figure 13. Figure 13a demonstrates the vertical downward deformation of the earth surrounding the foundation pit, which increases and subsequently diminishes as one moves away from the pit. The surface settling is depicted to be moving away from the foundation pit in Figure 13b. The greatest surface settlement, which is located at the surface 5 m from the side of the foundation pit and is 11.34 mm, can be observed in Figure 13b. Thereafter, the surface settlement steadily declines in the direction away from the foundation pit until it reaches zero.

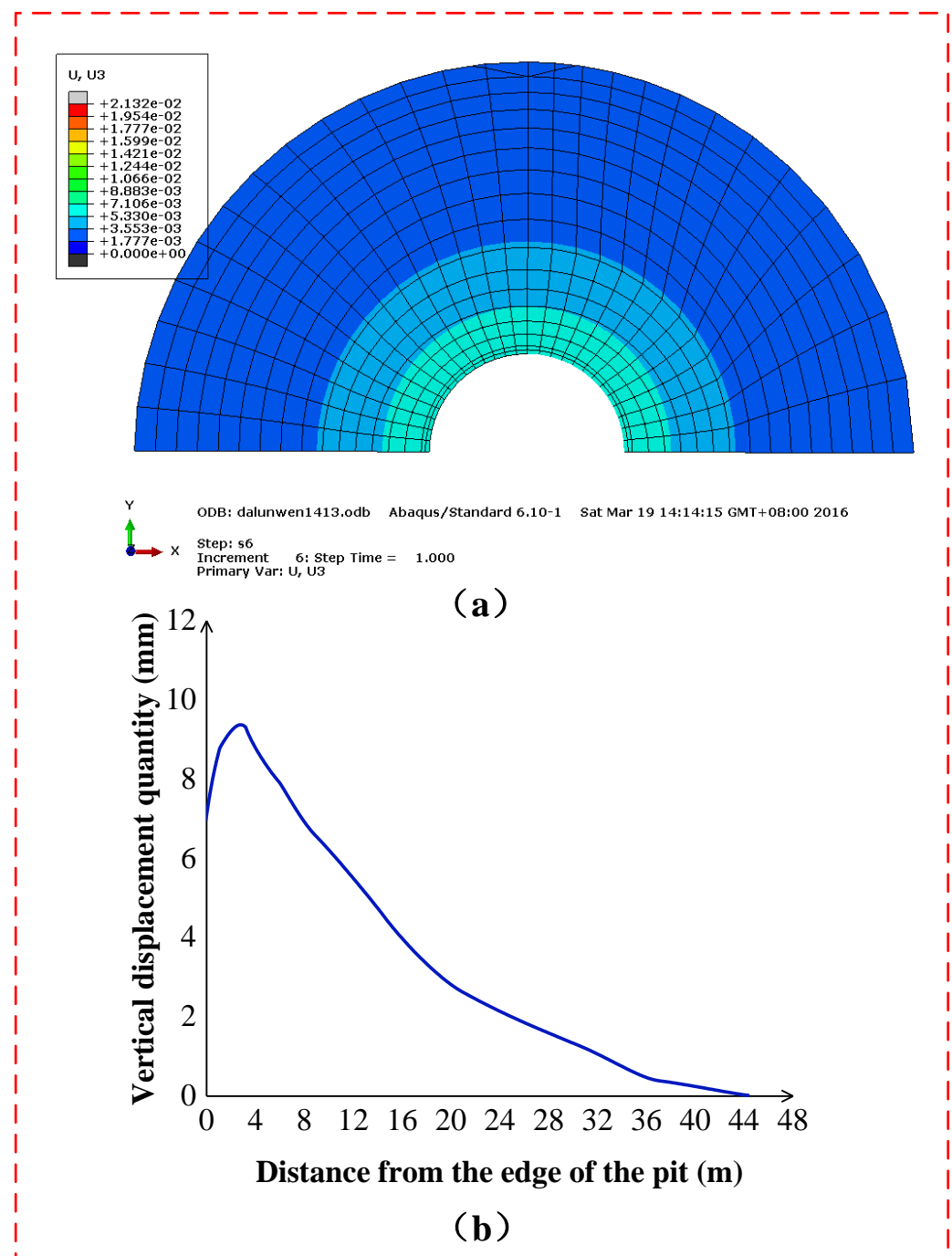


Figure 13. Surface subsidence: (a) vertical displacement cloud of the earth's surface; (b) surface settlement map.

4.2.4. Stress Analysis of Foundation Pit

Figure 14 illustrates how the soil stress of the soil model far from the foundation pit grows with depth, whereas the soil stress within the foundation pit's impact range varies near the diaphragm wall, and the effect decreases with distance from the foundation pit. The soil surface has the lowest stress, while the soil mass's maximum stress from gravity is 280.13 MPa. The diaphragm wall's stress distribution is maximum at the toe of the wall, where the stress value is 838.72 MPa. The diaphragm wall's stress value, which results from the foundation pit's excavation, is higher than the soil's due to its weight, and it typically rises with depth and exceeds the soil's stress value at an equal height.

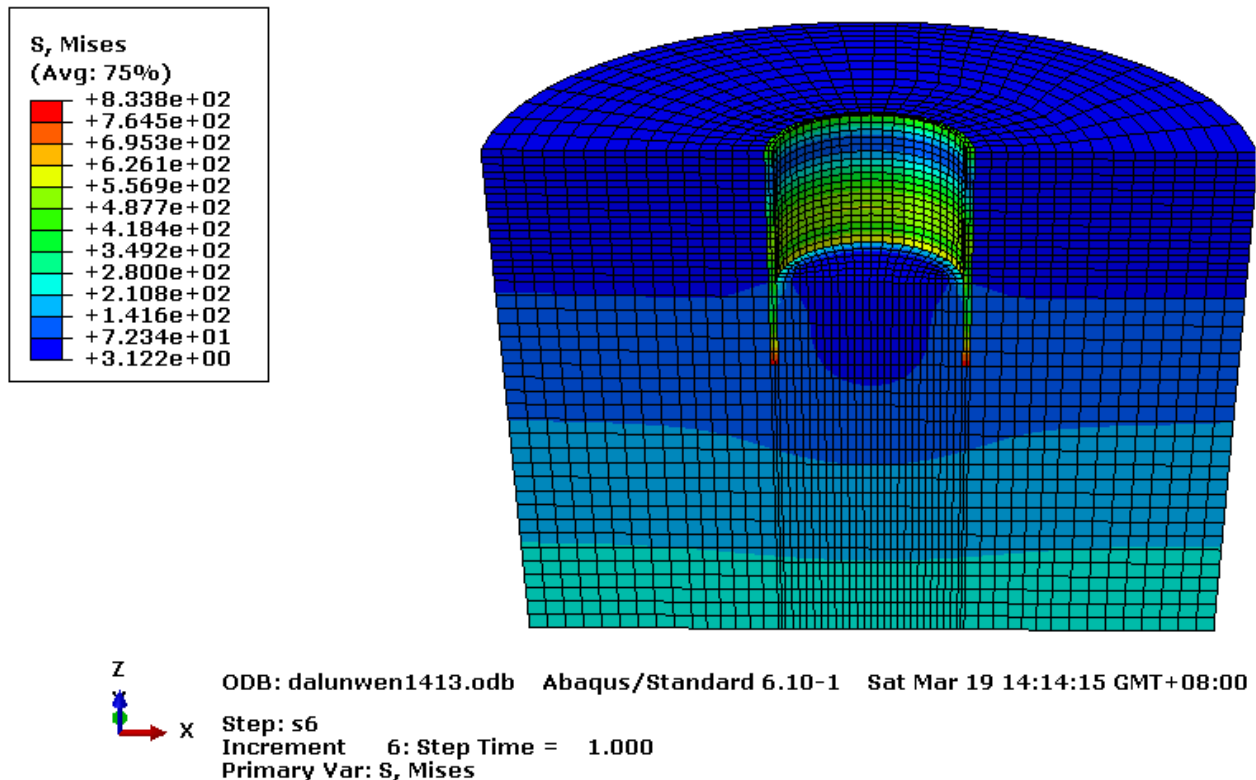


Figure 14. Stress plot after excavation of the foundation pit.

4.2.5. Analysis of Numerical Simulation Results of Diaphragm Wall in Foundation Pit Project

The lateral displacement program and lateral displacement map of the diaphragm wall following excavation are shown in Figure 15a,b. The program shows that the abdomen is where the diaphragm wall's maximum lateral displacement occurs, whereas the horizontal displacement of the toe and top of the wall is minimal; the maximum lateral displacement is 6.23 mm, and the top lateral displacement is minimal, 2.27 mm; the entire arrangement is a parabola combination. The total study reveals that the circular foundation pit diaphragm wall support has good safety since the lateral displacement of the diaphragm wall support is minimal.

Figure 15c,d shows the stress cloud diagram and stress coordinate diagram of the diaphragm wall after the excavation of the foundation pit. The figure shows that, following the excavation of the foundation pit, the stress at the toe of the diaphragm wall is at its highest level and has a value of 838.72 MPa; the stress at the top of the wall is at its lowest level and has a value that is very near 0 MPa. The diaphragm wall's stress is dispersed in an "S" pattern.

Figure 16a depicts the diaphragm wall's horizontal displacement following the excavation of each soil layer in the foundation pit. The graphic shows how the distortion of continuous walls steadily worsens with the foundation pit excavation. The diaphragm wall gradually changes from a cantilever-type lateral displacement during the excavation of the

first and second soil layers of the foundation pit to a parabolic-type lateral displacement after the excavation of the third soil layer. The lateral displacement in the abdomen of the diaphragm wall is the largest, while the displacement at the top of the wall is smaller. After each layer has been excavated, the underground diaphragm wall's stress distribution diagram is shown in Figure 16b. Following the first layer's excavation, the underground diaphragm wall's minimum stress is near 0 MPa at its top, and its highest stress is 63.12 MPa at its toe. The tension on the diaphragm wall grows over time as the foundation pit is continuously excavated, yet it is highest at the toe and lowest at the top of the wall. The greatest value is 838.72 MPa, and the minimum value is almost 0 MPa up until the end of the excavation. Thus, it is evident that the maximum value varies during the foundation pit excavation procedure. As can be seen, the excavation process has a maximum variance range of 63.12 MPa to 838.72 MPa at the wall's toe, while the minimum value is consistently 0 MPa at the wall's top.

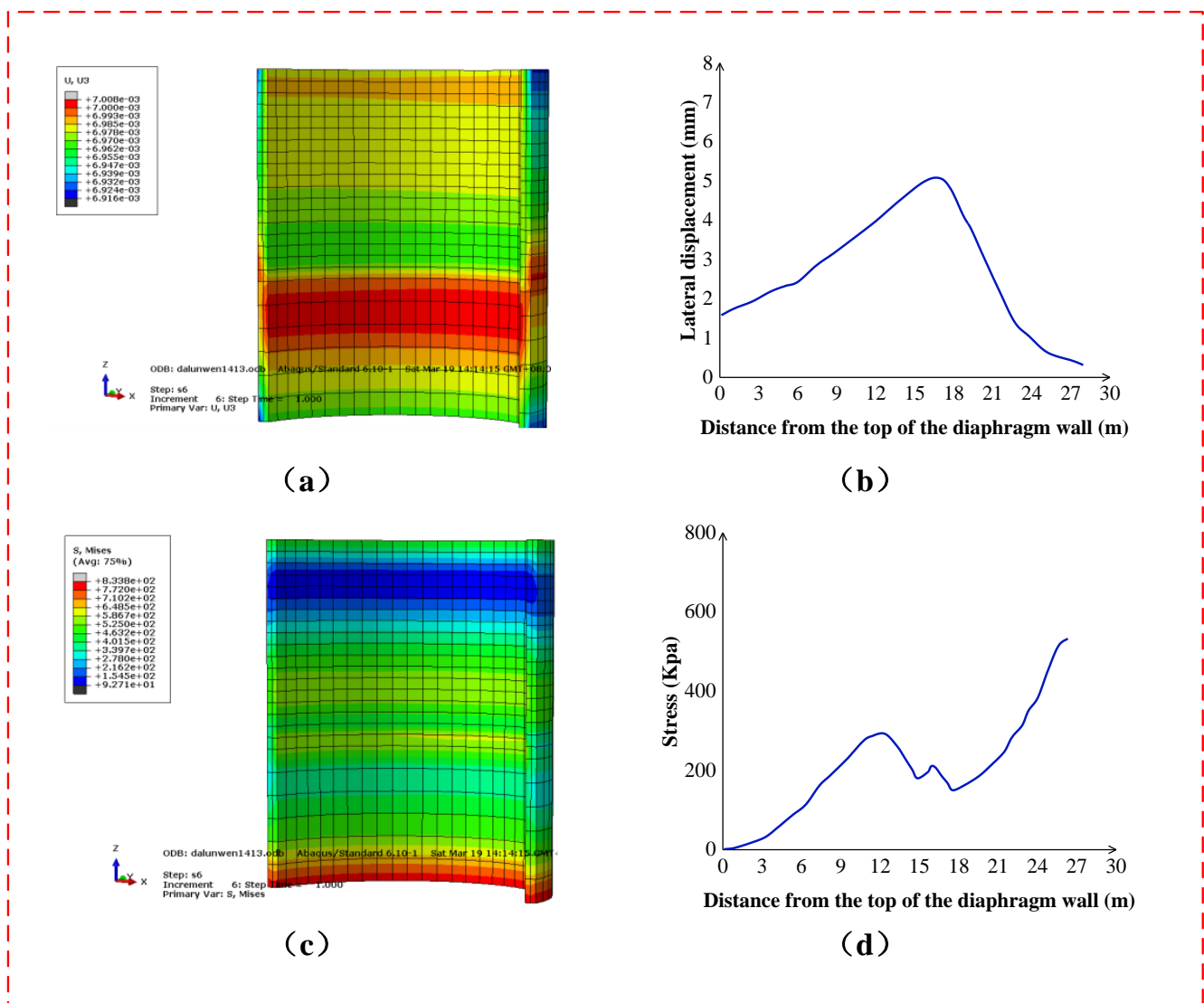


Figure 15. Lateral displacement diagram and stress map after excavation of a continuous underground wall: (a) lateral displacement cloud map of underground diaphragm wall; (b) lateral displacement coordinate map of underground diaphragm wall; (c) stress cloud map of underground diaphragm wall after excavation; (d) stress coordinate map of underground diaphragm wall after excavation.

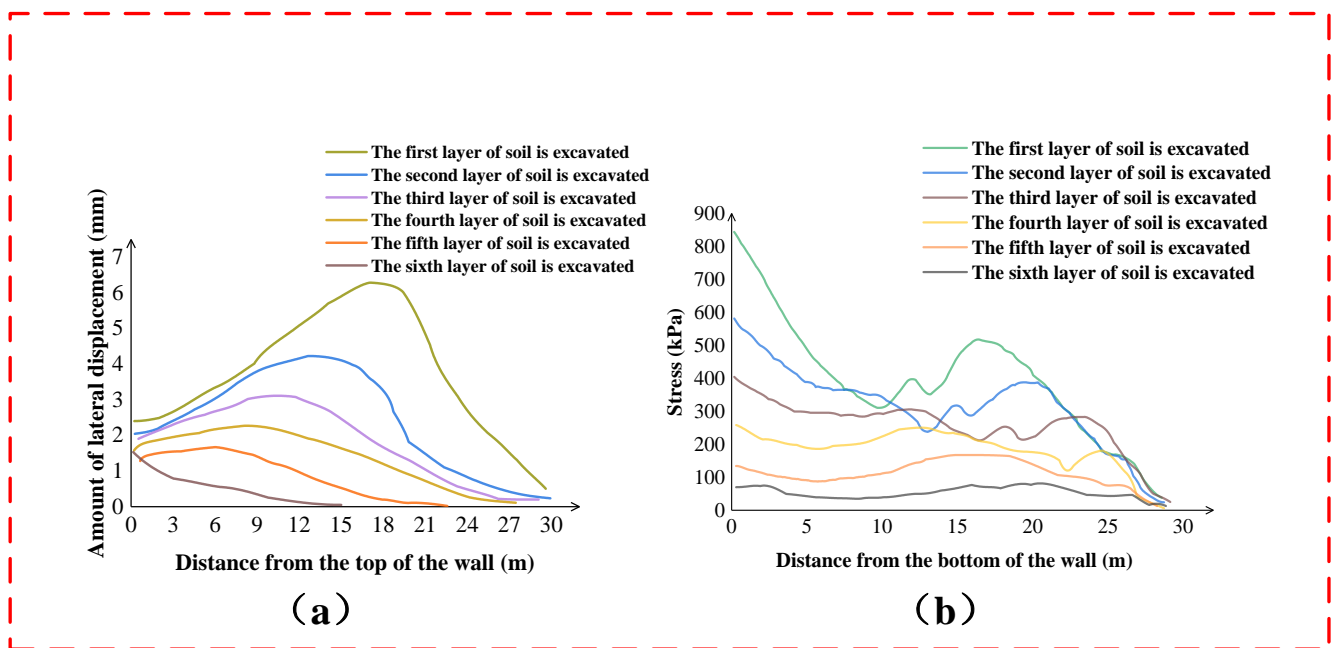


Figure 16. Comparison diagram of lateral displacement and stress of a continuous underground wall: (a) lateral displacement comparison diagram of underground diaphragm wall; (b) stress comparison diagram of underground diaphragm wall after excavation.

5. Comparison of Calculation Results

The calculation results for the foundation pit support differ between the plane elastic foundation beam method and the numerical simulation of the Abaqus program because they use distinct calculation philosophies. The comparison between the two calculation findings for this foundation pit project is shown in Table 1:

Table 1. Numerical simulation compared with foundation beam method calculation results.

	Abaqus Software Calculates the Results	Calculation Results of the Foundation Beam Method
The horizontal maximum displacement of an underground continuous wall	6.23 mm	4.70 mm
Deformed form of underground continuous wall	Parabola	Parabola
The foundation pit is raised	The maximum bulge is 23.4 mm	Meets the anti-uplift test
Maximum surface settlement	11.34 mm	8 mm

Table 1 shows that the results of the analysis performed by the Abaqus software and the calculations made using the foundation beam method are consistent, i.e., they both involve parabolic combinations, and the results of the calculation performed by the Abaqus software for the horizontal maximum displacement of a continuous underground wall are higher than those made using the foundation beam method. The foundation beam method immediately calculates the anti-uplift coefficient for the computation of the uplift at the bottom of the pit following the excavation of the foundation pit to see whether it complies with the stability criteria. According to the Abaqus software's estimate, the elastic uplift has an upper limit of 0.21 m, which satisfies engineering requirements. The foundation beam method calculates the three different types of surface settlement; the maximum settlement amount for parabolic settlement is 8 mm, while the maximum settlement amount for surface settlement determined by Abaqus software is 11.34 mm. The settlement pattern is that the amount increases initially in the direction away from the foundation pit, reaches the periphery, and then decreases.

The investigation shows that, when the arch effect is taken into account, the Abaqus software calculation result is superior to that of the elastic technique. Without taking the spacing effect into account, calculation results are often secure. However, the project uses the flat elastic foundation beam approach, which has small calculation results since it takes the spacing impact into account. The safety reserve of the design must be taken into account while utilizing this method to create designs.

6. Conclusions

For the research object, an underground granary project, first calculate the plane elastic foundation beam of the foundation pit while considering the arch effect. Then, using Abaqus, conduct numerical simulation analysis, analyze the soil displacement analysis and foundation pit deformation, and conduct stress analysis on the continuous underground wall displacement in each construction stage of the foundation pit excavation, and compare the results with the previous checks:

(1) The maximum displacement is 4.7 mm in the middle of the diaphragm wall; the maximum shear force is 129.36 kN in the middle of the diaphragm wall; the maximum bending moment is 279.25 kN*m; and the maximum is also situated in the middle of the diaphragm wall. This calculation result was obtained for the diaphragm wall structure, taking the arch effect into account.

(2) The entire foundation pit project is numerically simulated using the Abaqus program, and the calculated outcomes are as follows: the foundation pit bottom can move up to 23.4 millimeters vertically, and as little as 7.1 millimeters; The largest amount of surface settlement, 11.34 mm, is found at the surface 5 meters from the side of the foundation pit, and it steadily declines with the direction away from the foundation pit until it reaches 0; Following the excavation of the foundation pit, the soil is under 280.13 MPa of stress from its gravity, with the soil surface experiencing the least amount of stress. The diaphragm wall has a maximum lateral displacement of 6.23 mm and a minor top lateral displacement of 2.27 mm. The diaphragm wall has a maximum lateral stress distribution with a stress value of 838.72 MPa at the toe of the wall. There is a parabolic lateral displacement overall.

(3) After comparison, the three-dimensional numerical simulation analysis results and the calculation results produced utilizing the planar elastic foundation beam method while taking the arch effect into account are within the project's permitted range. In engineering practice, the planar elastic foundation beam approach that takes the arch effect into account is utilized to calculate costs. Consider utilizing Abaqus numerical simulation to estimate the types and risk components of potential dangers in advance and suggest suitable safety construction solutions if you want to see the force deformation of the structure in the latter stage of continuous underground wall support.

By changing the thickness and buried depth parameters of the diaphragm wall, the construction scheme is optimized, which provides a reference for the deep foundation pit support mode of a similar diaphragm wall.

Author Contributions: Conceptualization, C.Z. and Y.F.; methodology, W.W.; software, Z.N.; validation, C.Z., Y.F. and W.W.; formal analysis, C.Z.; investigation, C.Z.; resources, Y.F.; data curation, W.W.; writing—original draft preparation, Z.N. All authors have read and agreed to the published version of the manuscript.

Funding: This research was funded by the Henan Provincial Development and Reform Commission [Grant No. Yufa Gaoji [2022] No. 315], the 2021 Higher Education Teaching Reform Research and Practice Project in Henan Province [Grant No. 2021SJGLX670], and Key scientific research projects of Henan Province colleges and universities in 2023 [Grant No. 23B570003].

Institutional Review Board Statement: Not applicable.

Informed Consent Statement: Not applicable.

Data Availability Statement: Not applicable.

Conflicts of Interest: The authors declare no conflict of interest.

References

1. Long, M. Database for Retaining Wall and Ground Movements due to Deep Excavations. *J. Geotech. Geoenviron. Eng.* **2001**, *127*, 203–224. [[CrossRef](#)]
2. Zhang, L.; Ying, H.; Xie, K.; Huang, D. Effect of Groundwater Fluctuations on Pore Pressures and Earth Pressures on Coastal Excavation Retaining Walls. *Mar. Georesour. Geotechnol.* **2016**, *34*, 770–781. [[CrossRef](#)]
3. Tan, Y.; Wang, D. Characteristics of a Large-Scale Deep Foundation Pit Excavated by the Central-Island Technique in Shanghai Soft Clay. II: Top-Down Construction of the Peripheral Rectangular Pit. *J. Geotech. Geoenviron. Eng.* **2013**, *139*, 1894–1910. [[CrossRef](#)]
4. Tan, Y.; Wei, B. Observed Behaviors of a Long and Deep Excavation Constructed by Cut-and-Cover Technique in Shanghai Soft Clay. *J. Geotech. Geoenviron. Eng.* **2012**, *138*, 69–88. [[CrossRef](#)]
5. Wang, J.H.; Xu, Z.H.; Wang, W.D. Wall and Ground Movements due to Deep Excavations in Shanghai Soft Soils. *J. Geotech. Geoenviron. Eng.* **2010**, *136*, 985–994. [[CrossRef](#)]
6. Yuan, B.; Chen, M.; Chen, W.; Luo, Q.; Li, H. Effect of Pile-Soil Relative Stiffness on Deformation Characteristics of the Laterally Loaded Pile. *Adv. Mater. Sci. Eng.* **2022**, *2022*, 4913887. [[CrossRef](#)]
7. Yuan, B.; Chen, W.; Zhao, J.; Li, L.; Liu, F.; Guo, Y.; Zhang, B. Addition of alkaline solutions and fibers for the reinforcement of kaolinite-containing granite residual soil. *Appl. Clay Sci.* **2022**, *228*, 106644. [[CrossRef](#)]
8. Yuan, B.; Chen, W.; Zhao, J.; Yang, F.; Luo, Q.; Chen, T. The Effect of Organic and Inorganic Modifiers on the Physical Properties of Granite Residual Soil. *Adv. Mater. Sci. Eng.* **2022**, *2022*, 9542258. [[CrossRef](#)]
9. Yuan, B.; Li, Z.; Chen, W.; Zhao, J.; Lv, J.; Song, J.; Cao, X. Influence of Groundwater Depth on Pile–Soil Mechanical Properties and Fractal Characteristics under Cyclic Loading. *Fractal Fract.* **2022**, *6*, 198. [[CrossRef](#)]
10. Li, L.; Wang, W.; Xu, Z.; Niu, Z.; Li, X.; Wang, Q.; Feng, D. Mechanical Property Test and Finite Element Simulation Analysis of KH-560 Coupling Agent-Modified PVA Rubber Concrete. *Geofluids* **2022**, *2022*, 2839755. [[CrossRef](#)]
11. Shaojun, W.; Jiangyun, L.; Lin, G.; Lin, S. Numerical analysis on frost heave deformation and control for retaining system of deep foundation pit. *China Civ. Eng. J.* **2018**, *51*, 122–128. [[CrossRef](#)]
12. Xueyuan, G.; Mingju, Z.; Dong, M.; Lixin, H.; Wuxian, W.; Chunsheng, W.; Shipeng, Y.; Jingsheng, Q. Case study on braced excavation with P-CFST for top internal support. *J. Zhejiang Univ. (Eng. Sci.)* **2019**, *53*, 51–60. [[CrossRef](#)]
13. Li, P.; Chen, J.; Lv, Y.; Wang, Z.; Chen, X. Numerical investigation of the influence of spatial effects and supporting structures during pit excavation. *Acta Geotech. Slov.* **2020**, *17*, 87–96. [[CrossRef](#)]
14. Dongxing, R.; Hai, H.; Kang, S.; Huanhuan, L.; Donglin, L.; Peng, X. Displacement and stress analysis of a Shanghai foundation pit at excavation stages. *Build. Struct.* **2022**, *52*, 116–124. [[CrossRef](#)]
15. Peidong, Z.; Xiang, P.; Guanghua, Y.; Zhiling, L.; Guolong, Q. Analysis of Optimum Design Scheme of Circular Shaft in Soil and Rock Combination Stratum. *Chin. J. Undergr. Space Eng.* **2022**, *18*, 252–259, 273.
16. Xu, L.; Jinming, X.; Shaofeng, L. Exploring factors influencing deformation of retaining structure in orthogonal tests. *J. Shanghai Univ. (Nat. Sci.)* **2019**, *25*, 1003–1012. [[CrossRef](#)]
17. Mingnian, W.; Zhengqiang, Z.; Yinting, Z.; Dagang, L.; Shengzhi, W. Study on deformation rules of earth’s surface and support structure for deep foundation pit in bad gradation pebble stratum. *J. Railw. Sci. Eng.* **2019**, *16*, 646–653. [[CrossRef](#)]
18. Yang, C.; Wen, Z.; Pengjiao, J.; Jian-yong, H. Stability Assessment and Mechanical Effects Analysis on Deep Foundation Pit in Sandy Soil. *J. Northeast. Univ. (Nat. Sci.)* **2018**, *39*, 1353–1357. [[CrossRef](#)]
19. Changjiang, W.; Zhaohua, S.; Yunjin, L.; Hua, B. Study of deformation characteristics of diaphragm wall induced by deep large excavation in soft soil region. *Rock Soil Mech.* **2018**, *39*, 245–253. [[CrossRef](#)]
20. Shaoheng, H.; Tangdai, X.; Lianxiang, L.; Bingqi, Y.; Zeyong, L. Influence of groundwater seepage on deformation of foundation pits with suspended impervious curtains. *J. Zhejiang Univ. (Eng. Sci.)* **2019**, *53*, 713–723. [[CrossRef](#)]
21. Yong, H.; Yunan, L.; Bo, L.; Cong-an, L.; Jiefu, X. Centrifugal model tests and numerical simulation of three-dimensional space effect of deep and large foundation pit under the confined water level fluctuation. *Rock Soil Mech.* **2018**, *39*, 1999–2007. [[CrossRef](#)]
22. Hongxin, W. Stability Analysis of Retaining Structure for Circular Foundation Pit. *Chin. J. Undergr. Space Eng.* **2011**, *7*, 1653–1659.
23. Fuqiang, C.; Guanghua, Y.; Yucheng, Z.; Lina, Y. Discussion on value of coefficient α in structural design of circular diaphragm wall. *Chin. J. Geotech. Cal Eng.* **2012**, *34*, 203–206.
24. Ming-qiang, M.; Ju-hua, X. Anti-overturning stability analysis of cement-soil gravity retaining wall under different earth pressure modes. *Chin. J. Geotech. Eng.* **2014**, *36*, 12–17. [[CrossRef](#)]

Disclaimer/Publisher’s Note: The statements, opinions and data contained in all publications are solely those of the individual author(s) and contributor(s) and not of MDPI and/or the editor(s). MDPI and/or the editor(s) disclaim responsibility for any injury to people or property resulting from any ideas, methods, instructions or products referred to in the content.